AGU PUBLICATIONS

Geophysical Research Letters

RESEARCH LETTER
10.1002/2014GL062534

Key Points:
- Cliff-top ground motions are observed under extreme wave conditions (H_s = 6–8 m)
- Under extreme wave conditions, vertical ground displacements were > 50–100 μm
- Storm induced erosion is 2 orders of magnitude larger than the long-term rate

Supporting Information:
- Readme
- Movie S1

Correspondence to:
C. S. Earlie,
claire.earlie@plymouth.ac.uk

Citation:
Earlie, C. S., A. P. Young, G. Masselink, and P. E. Russell (2015), Coastal cliff ground motions and response to extreme storm waves, *Geophys. Res. Lett.*, *42*, 847–854, doi:10.1002/2014GL062534.

Received 17 NOV 2014
Accepted 14 JAN 2015
Accepted article online 16 JAN 2015
Published online 12 FEB 2015

Coastal cliff ground motions and response to extreme storm waves

Claire S. Earlie[1], Adam P. Young[2], Gerd Masselink[1], and Paul E. Russell[1]

[1]School of Marine Science and Engineering, Plymouth University, Plymouth, UK, [2]Integrative Oceanography Division, Scripps Institution of Oceanography, University of California, San Diego, La Jolla, California, USA

Abstract Coastal cliff erosion from storm waves is observed worldwide, but the processes are notoriously difficult to measure during extreme storm wave conditions when most erosion normally occurs, limiting our understanding of cliff processes. Over January–February 2014, during the largest Atlantic storms in at least 60 years with deepwater significant wave heights of 6–8 m, cliff-top ground motions showed vertical ground displacements in excess of 50–100 μm; an order of magnitude larger than observations made previously. Repeat terrestrial laser scanner surveys over a 2 week period encompassing the extreme storms gave a cliff face volume loss of 2 orders of magnitude larger than the long-term erosion rate. The results imply that erosion of coastal cliffs exposed to extreme storm waves is highly episodic and that long-term rates of cliff erosion will depend on the frequency and severity of extreme storm wave impacts.

1. Introduction and Background

Wave pressure fluctuations on the ocean floor generate microseismic ground motions both at the coast and hundreds of kilometers inland. Seismologists and oceanographers have used this ocean-driven microseismic activity as a proxy for hindcasting wave climate [*Zopf et al.*, 1976; *Tillotson and Komar*, 1997] since as far back as the 1930s [*Gutenberg*, 1931; *Ramirez*, 1940; *Longuet-Higgins*, 1950]. More recently, combined observations of coastal ground motions and in situ nearshore hydrodynamic data have advanced our understanding of ground motion on different coastal morphologies and shelf bathymetries under varying tidal and wave conditions [*Adams et al.*, 2002, 2005; *Young et al.*, 2011, 2012, 2013; *Dickson and Pentney*, 2012; *Norman*, 2012; *Brain et al.*, 2014]. In most instances, considered cliff-top ground motions increase with increasing wave height and tidal elevations.

The cliff-top ground motions generated from local ocean waves can be categorized into three major frequency bands: (1) high frequency (HF) 1–50 Hz (1–0.02 s), reflecting the natural frequency of the ground as it "rings" in direct response to wave impact and breaking waves [*Young et al.*, 2013]; (2) low-frequency cliff motion or "flexing" generated by individual sea swell or single-frequency waves (SF) 0.1–0.05 Hz (10–20 s) [*Adams et al.*, 2005]; and (3) infragravity waves (IG) < 0.05 Hz (>20 s) [*Young et al.*, 2011, 2012] which load the foreshore, causing pressure fluctuations. Microseisms are also detected, and motions at double frequencies (DF, twice the primary sea swell frequency) (0.1–0.2 Hz, 1–5 s) exhibit similar amplitude at the coast and tens of kilometers inland [*Young et al.*, 2011, 2013; *Norman*, 2012].

Cliff-top ground motions measured in wave conditions with significant wave height H_s less than 3 m show vertical ground displacements in the region of 0.5–10 μm during each wave loading cycle [*Adams et al.*, 2005; *Young et al.*, 2011, 2013]. It has been suggested that this repetitive flexure of the cliffs ultimately fatigues rock strength and leads to cliff failure [*Adams et al.*, 2005]. Experiments using cross-shore seismometer arrays show an exponential decay in the ground motion signal (in the IG and SF bands) with distance inland [*Adams et al.*, 2005; *Young et al.*, 2011, 2012; *Norman*, 2012]. The stresses created by the decrease of displacement inland are thought to be responsible for potentially weakening the integrity of the rock structure [*Adams et al.*, 2005]. *Brain et al.* [2014] examined this hypothesis in sedimentary cliffs capped with glacial till deposits under a range of wave conditions (H_s < 5 m) and argued that "background" microseismic cliff-top motion caused by cyclical loading is usually not of sufficient amplitude to drive the growth of microcracks. However, *Brain et al.* [2014] also suggest that larger displacements associated with episodic wave events (H_s > 5 m) can be responsible for less frequent, cliff-normal displacements, leading to an interaction between groups of microcracks that could ultimately damage the integrity of the rock structure.

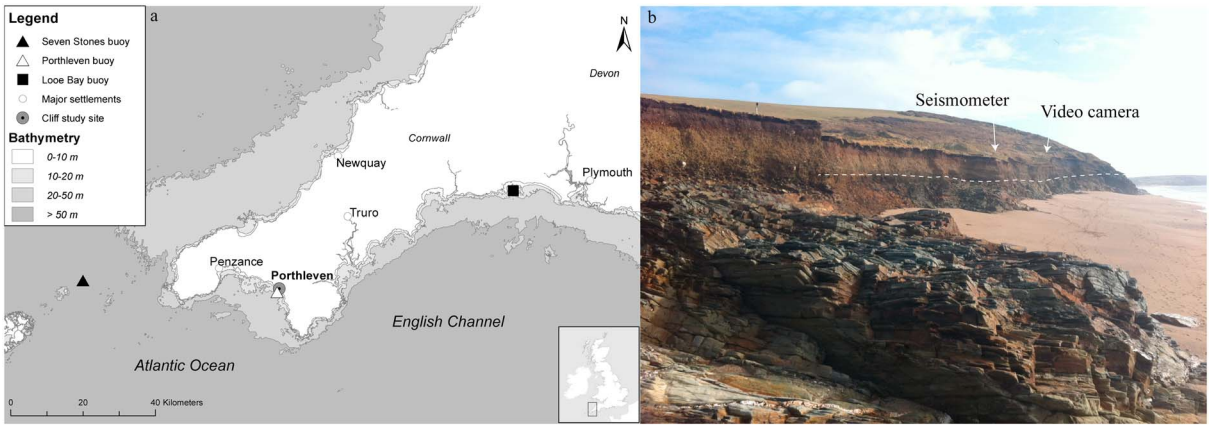

Figure 1. (a) Study site with locations of nearshore and deepwater wave buoys. (b) Photograph of the site and locations of seismometer and video camera. The boundary between the two major geological units (Mylor slates and overlying Quaternary head deposits) is identified with a dotted line. Mylor Slate characteristics are shown in the outcrop in the foreground.

Previous studies primarily focus on low to moderate incident ocean wave conditions, and observations of the impacts of extreme wave events are rare. This study describes a unique set of observations made during exceptionally energetic storm conditions on a coastal cliff in the southwest UK (occurring 31 January to 6 February 2014). The winter of 2014 was one of the most energetic periods the region has seen since the 1950s [*National Oceanic and Atmospheric Administration (NOAA)*, 2014] and brought over 10 storms with significant wave heights in excess of 6 m (the 1% exceedance limit). This study relates cliff-top seismic observations to visual observations of storm wave activity using both in situ and remote instrumentations. The cliff-top observations are placed in a longer-term context by comparing cliff-face changes that occurred over this extremely energetic period, obtained from terrestrial laser scanning, with the annual cliff-face development over the last 50 years.

1.1. Study Site

The study site (Figure 1) is situated on the southwest peninsula of the UK along a 300 m stretch of uninhabited cliffed coastline southeast of Porthleven, UK. Facing southwest toward the Atlantic Ocean, the site is subject to a highly energetic wave climate, being exposed to both locally generated wind waves and Atlantic swell from the south and southwest [*Scott et al.*, 2011]. The tidal regime is macrotidal with a mean spring range of 4.7 m. The cliffs are fronted by a steeply sloping (slope 0.12) beach, formed mainly of flint of two classes: coarse to very coarse sand (1–2 mm) and fine to medium gravel (2–16 mm) [*Buscombe and Scott*, 2008]. The cliffs rise 8–10 m above the beach, and the beach elevation at the cliff toe varies from anywhere between 2 m and 4 m seasonally (in Ordnance Datum Newlyn, which is ~0.2 m above mean sea level).

The cliffs are mainly formed of Late Devonian Mylor slate lithofacies and comprise of pale grey-green mudstone with interbedded siltstone and fine-grained sandstone [*Leveridge and Shail*, 2011]. The cliffs are oriented at 200°, dipping gently southeastward, and exhibit evidence of deformation during the Variscan Orogeny [*Alexander and Shail*, 1996]; cut by a variably reactivated network of Late Carboniferous-Triassic fractures, joints and faults steeply dipping SSW and NNE (Figure 1b). The Mylor slates are overlain by an ~2 m thick Quaternary head deposit of poorly consolidated clay, silt, sand, and gravel capped with a thin layer of "made ground" (0.3–0.5 m); a remnant of mining activity in the late nineteenth century [*Cornwall County Council*, 1999].

2. Methods

2.1. Wave Climate

Deepwater wave conditions were obtained from the Seven Stones offshore light vessel located 55 km to the west of the site with a water depth of approximately 60 m [*NOAA*, 2014]. Hourly statistics of offshore significant wave height were derived for the 7 day deployment duration. An inshore wave buoy located 1 km offshore (Porthleven buoy; Figure 1a) worked for the first 5 days of the deployment but malfunctioned following the exceptionally large waves on the night of 4 February. In order to extend the Porthleven wave record, the closest alternative inshore buoy situated 70 km ENE from the study site (Looe Bay directional wave

buoy deployed in ~10 m water depth; Figure 1a) was used. Over the available data period (2011–2014), significant wave heights at the Looe Bay buoy under southerly and southwesterly swell directions (180–225°) were only 5% smaller than the wave height measured at the Porthleven wave buoy. The inshore Looe Bay wave data were therefore considered representative for the wave conditions at Porthleven and were deshoaled using linear wave theory to obtain deepwater wave conditions. The deepwater significant wave height (H_s) and peak wave period (T_p) were subsequently used to compute the deepwater wave energy flux (P) using [*Komar*, 1998; *Masselink et al.*, 2011]

$$P = \frac{1}{16}\rho g {H_s}^2 C_g \tag{1}$$

where ρ is the density of seawater (1025 kg/m^3), g is the gravitational acceleration (9.81 m/s^2), and C_g is the deepwater group wave speed:

$$C_g = \frac{1}{2}\left(\frac{gT_p}{2\pi}\right) \tag{2}$$

2.2. Video Capture

The slightly embayed nature of the cliffs provided a promontory from which a GoPro® waterproof video camera inside a closed-circuit television casing was deployed, facing north alongshore, toward the cliffs. The videos were GPS time synced and closely inspected for cliff collapses, large wave impacts, and wave overtopping events for a 4:30 h period as the tide dropped from high tide to midtide during the most energetic storm wave event (5 February 2014). The video camera provided a qualitative, but detailed account of the hydrodynamics during the seismometer deployment.

2.3. Cliff-Top Ground Motion

The cliff-top ground motion was recorded using a Nanometrics Compact Trillium broadband seismometer sampling at 100 Hz. The seismometer response has 3 dB corners at 0.0083 and 108 Hz. The instrument was buried in the Quaternary deposit in the cliff-top about 1 m below the ground surface, 5 m from the cliff edge. The coastal cliff-top ground motions were compared with data obtained from the British Geological Survey inland broadband seismometer located at Carmellis, Cornwall, 17 km inland from the site, sampling at 50 Hz [*Observatories and Research Facilities for European Seismology*, 2014].

2.4. Seismic Data Processing

The raw ground vertical velocity data from the seismometer were corrected for phase and magnitude according to the instrument response curve. Hourly segments were band passed in the frequency domain to investigate ground motions over three frequency bands: high frequency (HF) 1–50 Hz, single frequency (SF) 0.1–0.05 Hz, and infragravity frequency (IG) 0.005–0.05 Hz. Double-frequency (DF) 0.1–0.2 Hz ground motions were also considered. The output velocity was integrated in the time domain to give ground displacement. Horizontal velocity data contain tilt effects at low frequencies [*Rodgers*, 1968; *Webb and Crawford*, 1999; *Crawford and Webb*, 2000] and have not been considered here.

2.5. Cliff-Face Volumes: Terrestrial Laser Scanning

Monthly scans of a 300 m cliff section at Porthleven were conducted using a Leica P20 terrestrial laser scanner over a 1 year period from July 2013 to July 2014 to enable linking the wave impacts on the cliff to cliff development. Volumetric changes at the cliff face were computed from these scans using a direct point-to-point cloud comparison method [*Lague et al.*, 2013].

3. Observations

3.1. Waves and Water Levels

The deepwater wave buoy data presented in Figure 2a show two exceptionally large storm wave events within our 7 day window. At this buoy location, the first storm on 1 February had larger waves than the second storm on 5 February ($H_s > 10$ m, $T_p > 14$ s, compared to $H_s > 8$ m and $T_p > 12$ s, respectively); however, the wave direction during the second storm was more southerly, delivering more wave energy to the Porthleven coast. This is confirmed by the inshore wave buoy statistics, which show more energetic wave conditions during the second storm ($H_s > 7$ m) compared to the first storm ($H_s > 5$ m). Maximum wave energy during both storms coincided with high tide (Figure 2a).

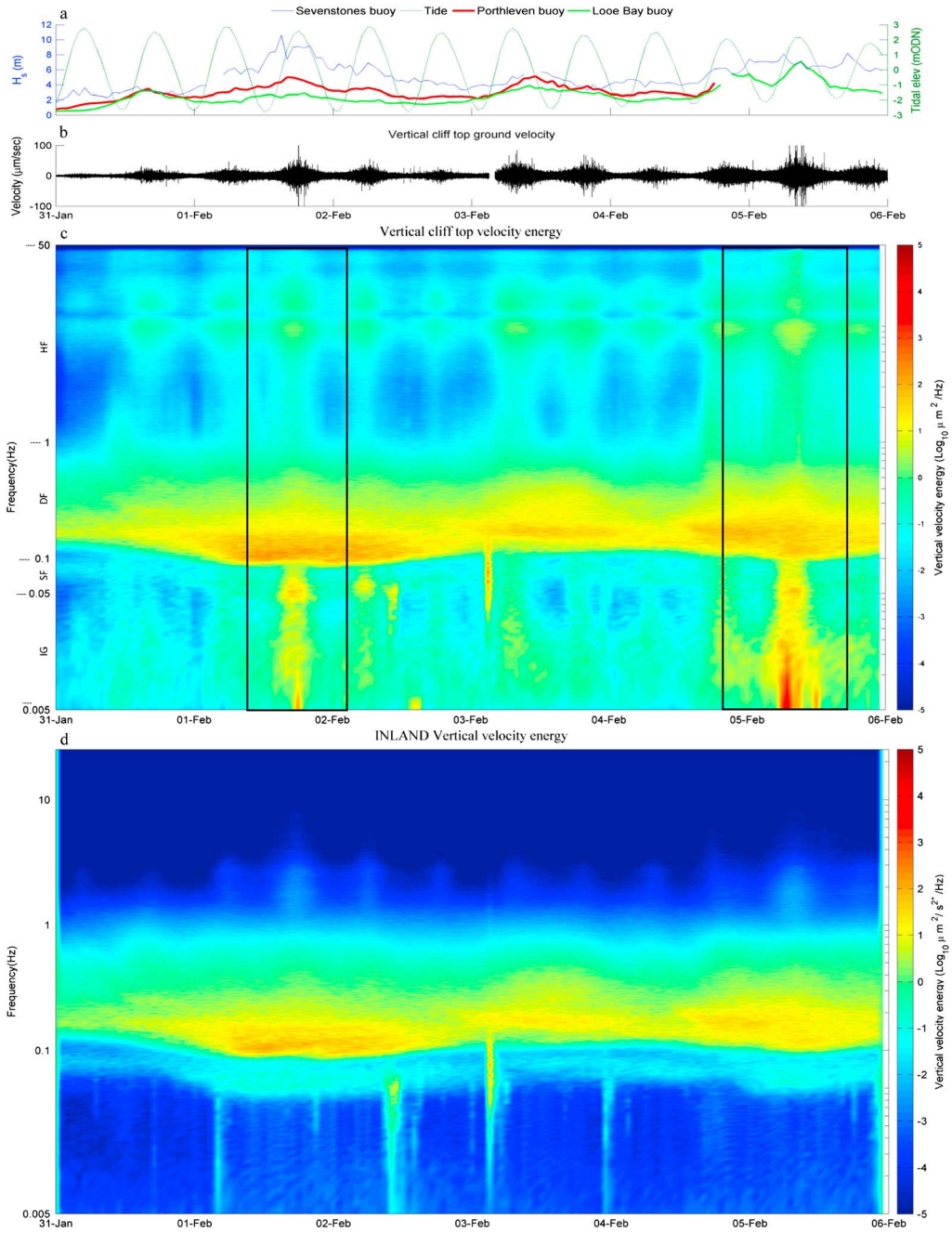

Figure 2. (a) Tidal elevations (predicted) and significant wave heights from offshore wave buoy (blue) nearshore wave buoy at Looe Bay (green) and recorded (solid red line) Porthleven wave buoy. (b) Time series of vertical cliff-top ground velocity. (c) Spectra of vertical cliff-top velocity energy and (d) spectra of vertical velocity energy inland. The two rectangles on the spectra denote the most energetic storm wave periods.

3.2. Cliff-Top Ground Velocities and Energy Spectra

The cliff-top ground velocities increased with increasing incident wave height and tide level (Figure 2b). The largest velocities occurred during the two extreme storm wave events on 1 and 5 February when significant wave heights offshore reached 6–8 m (Figure 2a).

Comparison with inland seismic vertical velocity energy data (Figure 2d) helped identify local and nonlocal sources of energy. Elevated HF signals were detected at the coast yet not inland, indicating a locally generated signal. The HF signals exhibited a tidal modulation and energy double peaks around 10 Hz and 20 Hz, suggesting

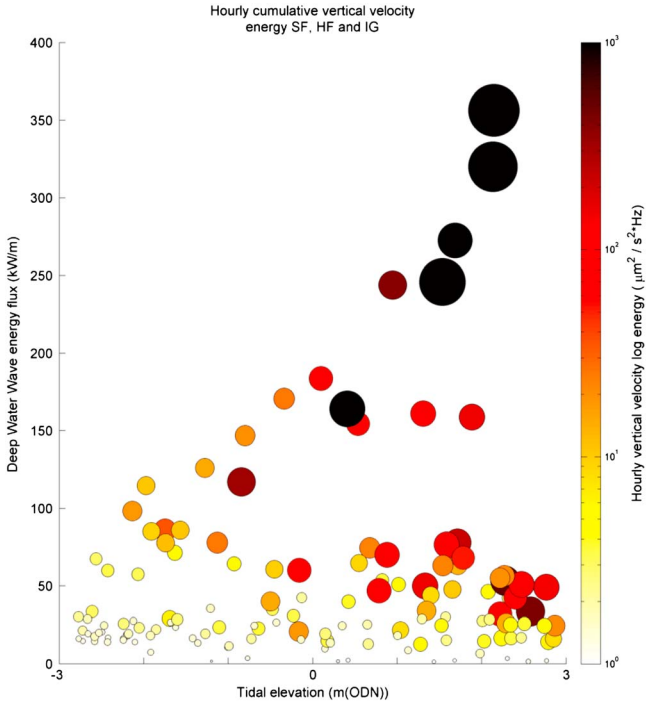

Figure 3. Hourly total log vertical velocity energy (between 50 and 0.005 Hz) excluding double frequencies (0.2–0.1 Hz) at various states of tide and deepwater wave energy flux (calculated using equations (1) and (2)). Vertical velocity energy is scaled by the color and size of the bubble and plotted logarithmically as the energy increases by orders of magnitude during the extreme events.

a possible primary normal site frequency of 10 Hz. Throughout the deployment, inland and coastal DF signals are similar suggesting a dominance of nonlocal signals at the coast, again, consistent with previous studies [i.e., *Young et al.*, 2013]. At the coastal site, elevated SF ground motions (not detected inland) coincided with the storm events. The inland seismometer detected three peaks in the infragravity-frequency range on 1, 2, and 4 February that were not detected at the coast, suggesting local inland source. The spectral peak located around 0.1 Hz on 3 February was present in both the inland and the coastal spectra and coincided with a magnitude 5.7 earthquake located at Lixourion, Greece [*U.S. Geological Survey*, 2014]. A clear IG energy peak occurred during the storm periods only in the coastal spectra (Figure 2c).

The total hourly vertical velocity energy is a function of both incident wave energy and the tidal elevation (Figure 3). Lower energy values are seen at all states of tide, yet only associated with lower wave energy flux ($<$100 kW/m). The highest velocity energy (an order of magnitude greater than "normal") only occurs during very energetic wave conditions and during higher tidal elevations (where cliff-top velocity energy exceeded 1000 $\mu m^2/s^2/Hz$ and wave power exceeded 200 kW/m). The largest contribution during energetic wave conditions and at higher tidal elevations is from energy at infragravity frequencies.

3.3. Displacements Under Extreme Wave Conditions

In previous cliff-top ground motion studies with significant wave heights up to 5 m, vertical displacements rarely exceeded 10 μm [*Adams et al.*, 2005; *Young et al.*, 2011, 2013]. At our site, ground displacements during both the extreme storm wave events increased by an order of magnitude (Figure 4b), where the vertical displacements increased from 5–10 μm under calmer periods to $>$50 μm under energetic conditions. These greatest vertical displacements occurred during the second storm event at high tide (Figures 2 and 4; from 08:00 on 5 February 2014).

The camera footage captured during the 5 February storm event shows different wave conditions including (1) wave breaking on the beach, (2) wave breaking at the cliff toe, and (3) overtopping of the entire cliff elevation. The timings of visible cliff collapses were also recorded (Figure 4a and Movie S1 in the supporting information).

Under energetic conditions, the largest vertical displacements (Figure 4b) were coincident with periods of successive cliff overtopping followed by water cascading down the cliff face. This suggests that wave loading and unloading on the cliff-top might significantly increase cliff motion and the associated strains and flexure mechanisms during times of wave overtopping at higher tidal elevations.

Peaks in IG and HF signals also coincided with time periods of successive overtopping and subsequent cascading events (Figures 4c and 4e at 08:15 and 09:05 h). However, not all overtopping events caused significantly elevated signals. Elevated SF signals occurred during some time periods of wave overtopping, but the signal variation was less clear compared to the timings of the peaks in the IG and HF signals.

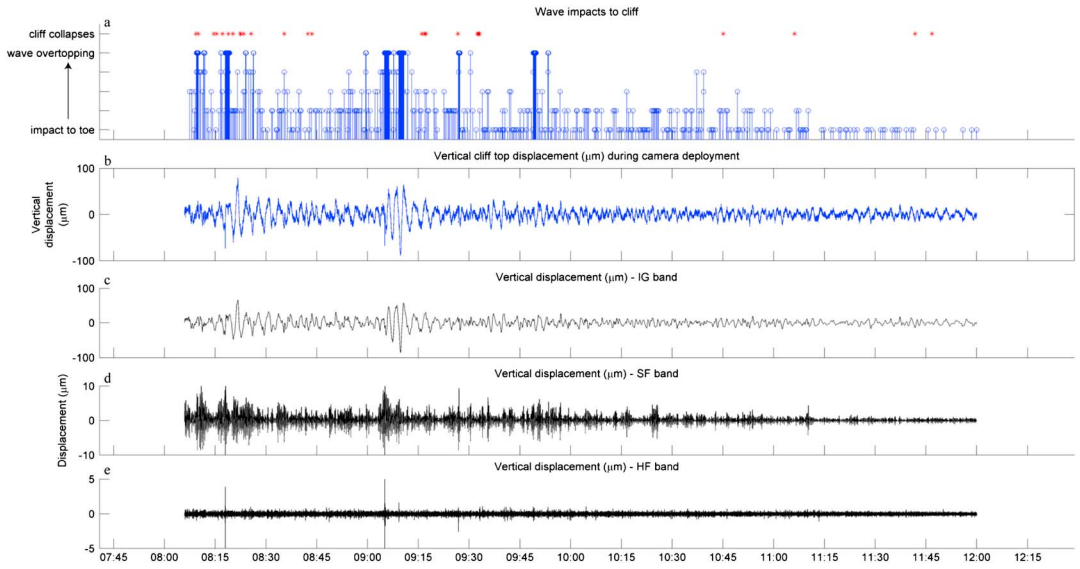

Figure 4. (a) Wave impacts to the cliff characterized using the video camera footage; *y* axis represents a gradual increase in height of wave impact up the cliff face, from impact to the toe to overtopping cliff-top. The red dots indicate the timings of cliff failures. The time series of vertical cliff-top displacement during camera deployment period (08:00 to 12:30 h on 5 February 2014): (b) across all frequency bands (0.005–50 Hz), (c) infragravity band IG (0.005–0.5 Hz), (d) single-frequency band SF (0.1–0.05 Hz), and (e) high-frequency band HF (1–50 Hz). High tide on 5 February occurred at 8:31 A.M.

During each overtopping event, the camera footage showed large volumes of water impacting the top of the cliff and cascading down the cliff face for a limited amount of time (from anywhere between 10 s to 2 min), the duration of which depended on the scale of overtopping (Figure 5a). The camera footage commenced 30 min prior to the peak of the high tide. Wave overtopping was recorded from this point and for up to 90 min after the peak of the tide. Although cliff collapses cannot be directly coupled with ground displacements, there appeared to be a period of time around the high tide where the majority of failures and wave overtopping occurred. Ground displacement increased in magnitude over this period of elevated tidal levels, suggesting that the cliff underwent an amplified series of strains and flexure mechanisms during times of wave overtopping. Although the timings of the intensive ground placements did not coincide exactly with the cliff failures, the period of energetic cliff motion coincided with the period of frequent cliff failures.

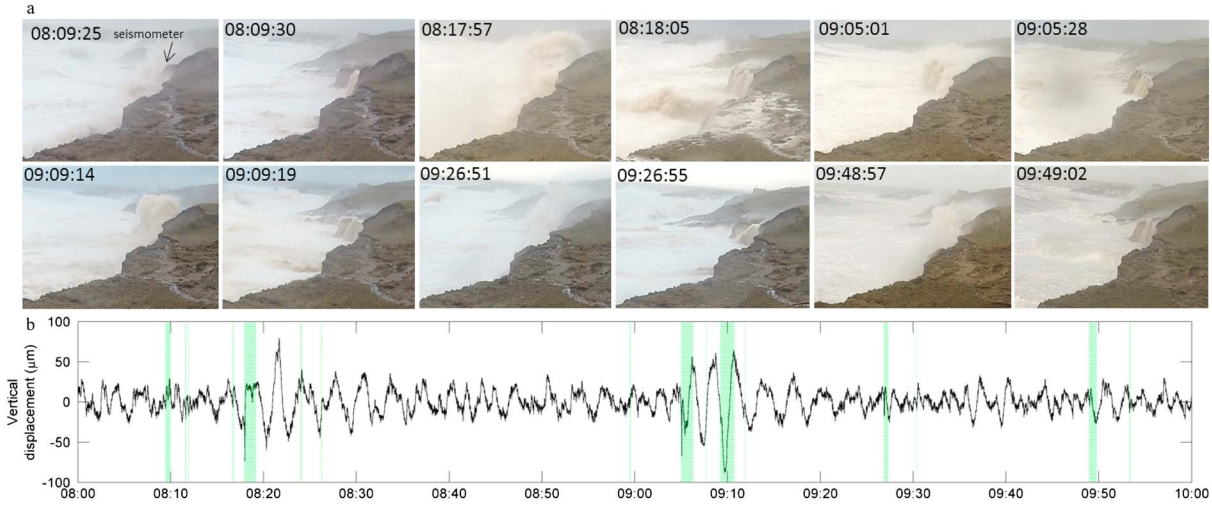

Figure 5. (a) Stills from camera footage illustrating successive wave overtopping and subsequent drainage events on 5 February 2014 from 08:09 to 09:49 h. (b) Vertical displacement during this period. The overtopped water cascading down the cliff face corresponds with the shaded regions of Figure 5b. A 60 s movie clip during the camera deployment is provided in Movie S1 in the supporting information.

4. Geomorphic Perspective and Relation to Cliff-Face Development

The consequences of these unusually large-scale cliff-top displacements (50–100 μm) under the largest wave conditions seen in 60 years in terms of rock damage from coastal flexing are unknown. However, previous research has suggested that although displacements under normal conditions are not likely to contribute toward the weakening of rock structures, episodic displacements caused by extreme wave conditions may be responsible for failure in metasedimentary cliffs [*Brain et al.*, 2014].

The long-term annual retreat rate for Porthleven, obtained from aerial photography and averaged over 50 years [*Ridgewell and Walkden*, 2009], is 0.1 m yr^{-1}. This value was corroborated by *Earlie et al.* [2014] using airborne lidar over a 3.5 year period (0.09 m yr^{-1}). Assuming a cliff height of 10 m, a long-term cliff recession rate of 0.1 m yr^{-1} equates to an annual cliff volumetric loss of 1 m^3 per meter length of cliff. Terrestrial laser scans over the 2 week storm period show that the 300 m long cliff section eroded 1350 m^3, which represents 4.5 m^3 average erosion volume per meter length of cliff over the 2 week period, or an annual cliff volumetric loss of 113 m^3 per meter length of cliff. The annual cliff volumetric loss over the 2 week storm period is therefore 2 orders of magnitude greater than volumetric loss based on the long-term cliff recession (i.e., 113 m^3 m^{-1} yr^{-1} versus 1 m^3 m^{-1} yr^{-1}).

During the 4.5 h camera deployment, the video footage clearly shows failure of cliff material throughout with over 30 failures recorded when energetic wave conditions and regular cliff overtopping prevailed; such cliff failure is not observed under calmer conditions, even at high tide. This strongly suggests that the observed cliff failures have been triggered by the direct combination of wave impacts and overtopping and possibly facilitated by the weakening of the cliff through microcrack density growth, such as suggested by *Adams et al.* [2005] and *Brain et al.* [2014]. The significance of these extreme wave events on erosion cliff morphology is further highlighted by the observation that the total erosion volume over the 2 week storm period not only exceeds the long-term erosion rate by 2 orders of magnitude but also accounts for more than half (53%) of the total volumetric loss for the years 2013–2014 with reportedly the most severe winter wave conditions on record.

5. Conclusions

Vertical cliff-top ground motions measured during an exceptionally stormy winter period in the UK were found to increase with increasing H_s and tidal elevation. During extreme wave conditions (H_s exceeding 6 m), vertical ground displacements increased by an order of magnitude from 10 μm to 100 μm. Real-time cliff-top video capture allowed for the association of these large ground displacements with the nearshore hydrodynamics and in particular cliff-top wave overtopping events. The greatest ground motion contribution (~100 μm) originated from displacements in the infragravity frequencies (0.5–0.005 Hz). The displacement peaks in the single frequencies (0.1–0.05 Hz) of 10 μm and high frequencies (1–50 Hz) of 5 μm also coincided with the timings of the wave overtopping events captured with the video camera. Cliff-face volume erosion measured over a 2 week storm period, encompassing the two extreme events discussed in this study, exceeded the long-term erosion rate by 2 orders of magnitude, providing a geomorphic link between energetic cliff-top ground displacements and cliff failure.

Capturing these events during one of the stormiest periods the region has seen in 60 years highlights the role that extreme events play in contributing toward coastal cliff erosion. Having recorded microseismic cliff-top motion on this scale for the first time and determined an effective method of monitoring the energetic wave impact in situ emphasizes how further investigation of cliff behavior during storms is not only obtainable but paramount to understanding coastal evolution under extreme conditions.

Acknowledgments

This work was funded by Plymouth University School of Marine Science and Engineering small research grant *Storm wave impacts on coastal cliffs*. Wave data are available from the Channel Coastal Observatory; inland seismic data from British Geological Survey; and coastal seismic data are available upon request from the authors. We gratefully thank Pedro Almeida, Tim Poate, Kit Stokes, Peter Ganderton, Robin Shail, and Mike Hardy for their invaluable field assistance under adventurous conditions.

The Editor thanks Mark Dickson and Patrick Barnard for their assistance in evaluating this paper.

References

Adams, P. N., R. S. Anderson, and J. Revenaugh (2002), Microseismic measurement of wave-energy delivery to a rocky coast, *Geology*, *30*, 895–898.

Adams, P. N., C. D. Storlazzi, and R. S. Anderson (2005), Nearshore wave induced cyclical flexing of sea cliffs, *J. Geophys. Res.*, *110*, F02002, doi:10.1029/2004JF000217.

Alexander, A. C., and R. K. Shail (1996), Late-to post-variscan structures on the coast between Penzance and Pentewan, south Cornwall, *Proc. Ussher Soc.*, *9*, 72–78.

Brain, M. J., N. J. Rosser, E. C. Norman, and D. N. Petley (2014), Are microseismic ground displacements a significant geomorphic agent?, *Geomorphology*, *207*, 161–173.

Buscombe, D. D., and T. M. Scott (2008), The coastal geomorphology of north Cornwall: St. Ives Head to Trevose Head, Wave Hub Impact on Seabed and Shoreline Processes (WHISSP), Univ. of Plymouth, Plymouth, U. K.
Cornwall County Council (1999), Cornwall Industrial Settlements Initiative: Porthleven, Historic Environment Service, Cornwall County Council.
Crawford, W. C., and S. C. Webb (2000), Identifying and removing tilt noise from low-frequency (<0.1 Hz) seafloor vertical seismic data, *Bull. Seismol. Soc. Am.*, *90*(4), 952–963.
Dickson, M. E., and R. Pentney (2012), Micro-seismic measurements of cliff motion under wave impact and implications for the development of near-horizontal shore platforms, *Geology*, *151–152*, 27–38.
Earlie, C. S., G. Masselink, P. E. Russell, and R. K. Shail (2014), Application of airborne LiDAR to investigate rates of recession in rocky coast environments, *J. Coast. Conserv.*, doi:10.1007/s11852-014-0340-1.
Gutenberg, B. (1931), Microseisms in North America, *Bull. Seismol. Soc. Am.*, *21*, 1–24.
Komar, P. D. (1998), *Beach Processes and Sedimentation*, 2nd ed., Prentice-Hall, Upper Saddle River, N. J.
Lague, D., N. Brodu, and J. Leroux (2013), Accurate 3D comparison of complex topography with terrestrial laser scanner: Application to the Rangitikei canyon (NZ), *ISPRS J. Photogramm. Remote Sens.*, *80*, 10–26.
Leveridge, B. E., and R. K. Shail (2011), The Gramscatho Basin, south Cornwall, UK: Devonian active margin successions, *Proc. Geol. Assoc.*, *122*, 568–615.
Longuet-Higgins, M. S. (1950), A theory of the origin of microseisms, *Philos. Trans. R. Soc.*, *243*, 1–35.
Masselink, G., M. G. Hughes, and J. Knight (2011), *Introduction to Coastal Processes and Geomorphology*, 2nd ed., Hodder Education, London.
National Oceanic and Atmospheric Administration (NOAA) (2014), National Oceanographic and Atmospheric Administration, National Data Buoy Centre, Station 62107–Sevenstones Lightship. [Available at http://www.ndbc.noaa.gov/station_page.php?station=62107], March.
Norman, E. C. (2012), Microseismic monitoring of the controls on coastal rock cliff erosion, PhD thesis, Department of Geography, Durham Univ.
Observatories and Research Facilities for European Seismology (2014), Observatories and research facilities for European Seismology, European Integrated Data Archive. [Available at http://145.23.252.222/eida/webdc3/], June.
Ramirez, J. E. (1940), An experimental investigation of the nature and origin of microseisms at St. Louis, Missouri, *Bull. Seismol. Soc. Am.*, *30*, 35–84, 139–178.
Ridgewell, J., and M. Walkden (2009), *Cornwall and Isles of Scilly SMP2 Sub-Cells Review of Coastal Processes and Geomorphology*, Royal Haskoning, Peterborough, U. K.
Rodgers, P. W. (1968), Response of horizontal pendulum seismometer to Rayleigh and Love waves tilt and free oscillations of Earth, *Bull. Seismol. Soc. Am.*, *58*(5), 1384–1406.
Scott, T., G. Masselink, and P. Russell (2011), Morphodynamic characteristics and classification of beaches in England and Wales, *Mar. Geol.*, *286*, 1–20.
Tillotson, K., and P. D. Komar (1997), The wave climate of the Pacific Northwest (Oregon and Washington): A comparison of data sources, *J. Coast. Res.*, *13*, 440–452.
U.S. Geological Survey (2014), Earthquake Hazards Program. [Available at http://comcat.cr.usgs.gov/earthquakes/eventpage/usc000mfuh#pager], October 2014.
Webb, S. C., and W. C. Crawford (1999), Long-period seafloor seismology and deformation under ocean waves, *Bull. Seismol. Soc. Am.*, *89*(6), 1535–1542.
Young, A. P., P. N. Adams, W. C. O'Reilly, R. E. Flick, and R. T. Guza (2011), Coastal cliff ground motions from local ocean swell and infragravity waves in Southern California, *J. Geophys. Res.*, *116*, C09007, doi:10.1029/2011JC007175.
Young, A. P., R. T. Guza, P. A. Adams, W. C. O'Reilly, R. E. Flick (2012), Cross-shore decay of cliff top ground motions driven by local ocean swell and infragravity waves, *J. Geophys. Res.*, *117*, C06029, doi:10.1029/2012JC007908.
Young, A. P., R. T. Guza, M. E. Dickson, W. C. O'Reilly, and R. E. Flick (2013), Ground motions on rocky, cliffed, and sandy shorelines generated by ocean waves, *J. Geophys. Res. Oceans*, *118*, 6590–6620.
Zopf, D. O., H. C. Creech, and W. H. Quinn (1976), The wavemeter: A land-based system for measuring nearshore ocean waves, *Mar. Tech. Soc. J.*, *10*, 19–25.